Automated Macromodelling of "Nonlinear" Wireless Blocks

Jaijeet Roychowdhury
jaijeet@research.bell-labs.com
Bell Laboratories, Murray Hill

Abstract

Behavioral modelling of blocks is an important step in wireless system verification. In this paper, we describe the application of an automated technique for macromodel extraction. Called TVP, the technique works directly from detailed transistor-level descriptions (e.g., SPICE) of a block to produce system-level macromodels (e.g., suitable for MATLAB). A key property of TVP is that it can reduce blocks with switching, sampling or frequency-translation properties. TVP is efficient for large circuits and can automatically tailor the size of the macromodel to meet a specified accuracy. TVP also produces dominant poles and zeros without need for lengthy simulations. We present applications to RF mixers and switched-capacitor filters, to obtain size reductions of more than two orders of magnitude with no appreciable loss of accuracy.

1 Introduction

An important task in communication system design is hierarchical verification of functionality at different levels, starting from individual circuits up to block representations of full systems. A key step in this process is the creation of small macromodels that abstract, to a given accuracy, the behaviour of much bigger subsystems. For systems with "nonlinear" blocks like mixers and switched-capacitor filters, this is typically achieved by using results from detailed nonlinear simulations to construct macromodels manually. This process has disadvantages. Nonlinear simulation does not provide parameters of interest (such as poles and zeros) directly; to obtain them by inspection, frequency-response plots with many points are often computed. This can be very time-consuming for large subsystems, since nonlinear blocks require a steady-state solution at each point. Also, the macromodelling step, critical for reliable verification, is heuristic, time-consuming and highly reliant on detailed internal knowledge of the system under consideration.

In this paper, we illustrate the use of a recently-developed algorithmic technique [Roy98c] for abstracting small macromodels from detailed descriptions of many kinds of "nonlinear" subsystems encountered in communication systems. Named TVP (Time-Varying Padé), the method reduces a large linear time-varying (LTV) system to a small one. The LTV model is adequate for many apparently nonlinear systems, like mixers and switched-capacitor filters, where the signal path is designed to be linear, even though other inputs (e.g., local oscillators, clocks) may cause "nonlinear" parametric changes to the system. The use of LTV descriptions is key, because they capture frequency translation and sampling/switching behaviour, unlike linear time-invariant (LTI) models.

TVP has several useful features. The computation/memory requirements of the method scale almost linearly with circuit size, thanks to the use of factored-matrix computations and iterative linear algebra [RA92, MFR95, RLF98]. TVP provides the reduced model as a LTI system followed by a memoryless mixing operation; this makes it easy to incorporate the macromodel in existing circuit and system level simulators. TVP itself can be implemented easily in a number of existing simulation tools, including nonlinear time-domain simulators like SPICE, nonlinear frequency-domain domain simulators using harmonic balance, as well as linear time-varying simulators like SWITCAP and SIMPLIS. Time-domain computations, moreover, do not necessarily require obtaining or using a steady state of the system. Existing LTI model reduction codes can be used as black boxes in TVP's implementation. Like its LTI counterparts, TVP based on Krylov methods is numerically well-conditioned and can directly produce dominant poles and residues.

Most importantly, by providing an automated means of generating reduced-order models to any desired accuracy, TVP enables macromodels of communication subsystems to be coupled to detailed realizations much more tightly and quickly than previously possible. This can significantly reduce the number of iterations it takes to settle on a final design.

In Section 2, we provide a brief description of how TVP works. The application of TVP to macromodel RF mixers and switched-capacitor filters is presented in Section 3.

2 Overview of TVP

In this section, we provide an overview of the TVP algorithm; a more detailed exposition may be found in [Roy98c]. The basic difficulty in formulating model-reduction techniques for LTV systems has been the interference of system time variations with input time variations. A key step in TVP is to separate the two time-scales, using recent concepts of multiple time variables and the MPDE [BWLBG96, Roy97a, Roy98a], resulting in forms for the LTV transfer function that are suitable for model reduction. Once the time scales have been separated, it becomes easy to obtain a useful expression for the LTV transfer function of the system.

We start with a nonlinear system described by a set of differential equations, such as those obtained from a SPICE-type description. We assume that the system driven by a large signal $b_l(t)$ and a small input signal $u(t)$, to produce an output $z_t(t)$. Let the differential equations of the circuit be:

$$\frac{\partial q(y(t))}{\partial t} + f(y(t)) = b_l(t) + bu(t), \quad z_t(t) = d^T y(t) \tag{1}$$

$y(t)$ is a vector of node voltages and branch currents; $q()$ and $f()$ are nonlinear functions describing the charge/flux and resistive terms, respectively, in the circuit. b and d are vectors that link the input and output to the rest of the system.

We now move to the MPDE (multirate partial differential equation [BWLBG96, Roy97a, Roy98a]) form of (1). Doing so enables the input and system time-scales to be separated and, as will become apparent, leads to a form of the LTV transfer function useful for reduced-order modelling. The move to the MPDE (2), below, is justified by the fact that (1) is exactly equivalent to (2).

$$\begin{aligned} &\frac{\partial q(\hat{y})}{\partial t_1} + \frac{\partial q(\hat{y})}{\partial t_2} + f(\hat{y}(t_1,t_2)) = b_l(t_1) + bu(t_2) \\ &\hat{z}_t(t_1,t_2) = d^T \hat{y}(t_1,t_2), \quad z_t(t) = \hat{z}_t(t,t) \end{aligned} \tag{2}$$

The hatted variables in (2) are bivariate (i.e., two-time) forms of the corresponding variables in (1).

To obtain the output component linear in u, we perform a linearization around the solution of (2) when $u(t_2) \equiv 0$. Let this solution be $\hat{y}^*(t_1)$ (note that we can always select $\hat{y}^*$ to be independent of t_2). Linearization about $\hat{y}^*$ yields the linear MPDE:

$$\begin{aligned} &\frac{\partial (C(t_1)\hat{x}(t_1,t_2))}{\partial t_1} + \frac{\partial (C(t_1)\hat{x}(t_1,t_2)))}{\partial t_2} + G(t_1)\hat{x}(t_1,t_2) = bu(t_2) \\ &\hat{z}(t_1,t_2) = d^T \hat{x}(t_1,t_2), \quad z(t) = \hat{z}(t,t) \end{aligned} \tag{3}$$

In (3), the quantities $\hat{x}$, $\hat{z}$ and z are the small-signal versions of $\hat{y}$, $\hat{z}_t$ and z_t, respectively; $C(t_1) = \frac{\partial q(\hat{y})}{\partial \hat{y}}\Big|_{\hat{y}^*(t_1)}$ and $G(t_1) = \frac{\partial f(\hat{y})}{\partial \hat{y}}\Big|_{\hat{y}^*(t_1)}$ are time-varying matrices.

Note that the bi-variate output $\hat{z}(t_1,t_2)$ is linear in the input $u(t_2)$, but that the relationship is time-varying because of the presence of t_1. To obtain the time-varying transfer function from u to $\hat{z}$, we Laplace

0-7803-5443-5/99/$10.00©1999 IEEE

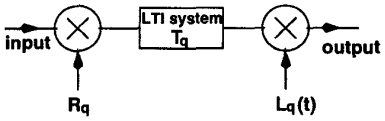

Figure 1: Specialized Floquet form of a LPTV system

transform (3) with respect to t_2:

$$\frac{\partial\left(C(t_1)\hat{X}(t_1,s)\right)}{\partial t_1} + sC(t_1)\hat{X}(t_1,s) + G(t_1)\hat{X}(t_1,s) = bU(s)$$
$$\hat{Z}(t_1,s) = d^T\hat{X}(t_1,s) \quad (4)$$

In (4), s denotes the Laplace variable along the t_2 time axis; the capital symbols denote transformed variables.

We can rewrite (4) as

$$\left(\frac{D}{dt_1}[\,] + sC(t_1) + G(t_1)\right)\hat{X}(t_1,s) = bU(s)$$
$$\hat{Z}(t_1,s) = d^T\hat{X}(t_1,s), \quad \text{where } \frac{D}{dt_1}[v] = \frac{\partial(C(t_1)v)}{\partial t_1} \quad (5)$$

and obtain an *operator form* of the time-varying transfer function $H(t_1,s)$:

$$H(t_1,s) = d^T\left(\frac{D}{dt_1}[\,] + sC(t_1) + G(t_1)\right)^{-1}[b], \hat{Z}(t_1,s) = H(t_1,s)\,U(s) \quad (6)$$

This LTV transfer function (6) is still in operator form, involving symbolic differentiation. The next step in TVP is to remove the operators, and cast the LTV transfer in terms of a number of linked LTI transfer functions. This step can be achieved using either frequency-domain techniques (*e.g.*, harmonics of the LO frequency) or time-domain ones (*e.g.*, samples of a clock signal). Once an equivalent system of LTI transfer functions has been obtained, TVP uses existing Padé approximation techniques for LTI systems to generate a reduced model that approximates the input-output relationship of the original, to any desired level of accuracy.

TVP has a number of useful properties:

- The reduced model produced by TVP has a special form known as the *Floquet form*, illustrated in Figure 1. In the Floquet form, the dynamics of the system are separated from the time-variation; hence the LTV system becomes equivalent to a LTI system, followed by a memoryless multiplication. This feature makes the reduced model very easy to incorporate in existing simulation tools, such as a SPICE or MATLAB model; furthermore, it also provides insight for hand-calculations with the reduced model, since the poles and zeros of the LTI block capture dynamics of the system. These poles and zeros can be obtained directly from eigenvalue analysis of the reduced model, without the need for transient simulations.
- Krylov-subspace algorithms such as Lanczos and Arnoldi, used for the reduction step of TVP, require matrix-vector multiplications, but no matrix inversions or direct linear system solutions. This property makes these computations scale almost linearly with the size of the circuit, since iterative linear algebra and factored-matrix methods (*e.g.*, [MFR95, TKW95, RLF98] are used. Thus the TVP algorithm is practical for reducing very large blocks.
- A system with several inputs and outputs can be macromodelled by TVP much more efficiently than by considering all combinations of input-output pairs. This is especially useful for, *e.g.*, simultaneous macromodelling of a system's transfer characteristics as well as its input and output driving point behaviour.

3 Application to wireless blocks

In this section, we present three applications of TVP. The first is a simple example, for the purpose of verifying TVP against hand calculations. The second is a RFIC upconverter consisting of an I-channel buffer and mixer. The third is a switched-capacitor integrator circuit. The latter two circuits were reduced directly from their extracted SPICE descriptions, together with information identifying the input sources and output nodes. The reduced model was produced for MATLAB, in which further calculations (like plotting transfer functions and computing poles) were performed.

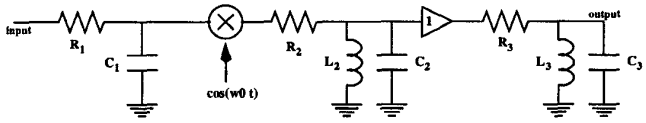

Figure 2: Lowpass filter→mixer→two bandpass filters

Original system	TVP, $q=2$	TVP, $q=3$
-4.98e3 - *j*3.88e3	-4.96e3 - *j*3.91e3	-4.98e3 - *j*3.88e3
-1.59e4 - *j*3.90e3	-1.56e4 - *j*3.49e3	-1.59e4 - *j*3.90e3
-9.95e4		-9.95e4
-5.72e4 - *j*2.00e7		
-3.59e4 - *j*1.99e7		

Table 1: Poles (Hz) of $H_1(s)$, original and reduced systems

3.1 A hand-calculable example

Figure 2 depicts an upconverter, consisting of a low-pass filter, an ideal mixer, and two bandpass filter stages. The component values were chosen to be: $R_1 = 160\Omega$, $R_2 = 1.6k\Omega$, $R_3 = 500\Omega$, $C_1 = C_2 = C_3 =$ 10nF, and $L_2 = L_3 = 25.35$nH. These values result in a low-pass filter with a pole at 100kHz, and band-pass filters with a center frequency of 10MHz and bandwidths of about 10kHz and 30kHz respectively. The LO frequency for the mixer was chosen to be 10Mhz.

The baseband-referred transfer functions of interest in this case are $H_1(s)$ and $H_{-1}(s)$ (the fundamental components of the time-varying transfer function), since they appear in the desired up- and down-conversion paths. It can be shown that $H_{-i}(s) = H_i^*(-s)$, hence it suffices to consider only $H_1(s)$ here. The expression for $H_1(s)$ can be derived easily using intuitive frequency-translation concepts; it is:

$$H_1(s) = \frac{0.5}{1+sC_1R_1}\,\frac{\frac{(s+j\omega_0)L_2}{1+(s+j\omega_0)^2L_2C_2}}{R_2+\frac{(s+j\omega_0)L_2}{1+(s+j\omega_0)^2L_2C_2}}\,\frac{\frac{(s+j\omega_0)L_3}{1+(s+j\omega_0)^2L_3C_3}}{R_3+\frac{(s+j\omega_0)L_3}{1+(s+j\omega_0)^2L_3C_3}} \quad (7)$$

(7) is plotted for positive and negative frequencies in Figure 3.1. Also plotted are the transfer functions obtained from TVP with $q = 2$ and $q = 3$. It can be seen that for $q = 2$, TVP produces a reasonable approximation, whereas for $q = 3$, the match is perfect, even though the original system is of order 5.

The poles of the original system and those from TVP are shown in Table 1. Note that the dominant pole is contributed by the lowpass RC filter at about 100kHz.

3.2 RFIC mixer block

Next, we apply TVP to a portion of the W2013 RFIC from Lucent Microelectronics, consisting of an I-channel buffer and mixer. The circuit consisted of about $n = 360$ nodes, and was excited by a local oscillator at 178Mhz driving the mixer, while the RF input was fed into the I-channel buffer. The time-varying system was obtained around a steady state of the circuit at the oscillator frequency; for this circuit, harmonic balance with $N = 21$ harmonics was used to find the steady-state operating point. Appropriately, a frequency-domain version of TVP was used for macromodelling this circuit.

Figure 3.2 shows frequency plots of $H_1(s)$, the upconversion transfer function. The points marked '+' were obtained by direct computation of the full system, while the lines were computed using the TVP-reduced models with $q = 2$ and $q = 10$, respectively. Even with $q = 2$, a size reduction of two orders of magnitude, the reduced model provides a good match up to the LO frequency. When the order of approximation is increased to 10, the reduced model is identical upto well beyond the LO frequency. Evaluating the reduced models was more than *three orders of magnitude faster* than evaluating the transfer function of the original system.

The poles of the reduced models for $H_1(s)$ are shown in Table 2.

3.3 Switched-capacitor integrator block

Our third application is macromodelling a switched-capacitor integrator block. The integrator is lossy, designed for Σ-Δ applications with a bandwidth of about 200kHz. The circuit was designed in a 0.35μ CMOS process, and modelled using a Lucent MOS model (ASIM3) specifically intended for high-accuracy analog simulations. Comprising more than 150 MOS devices, it includes biasing, common mode feedback and slew-rate enhancement sections.

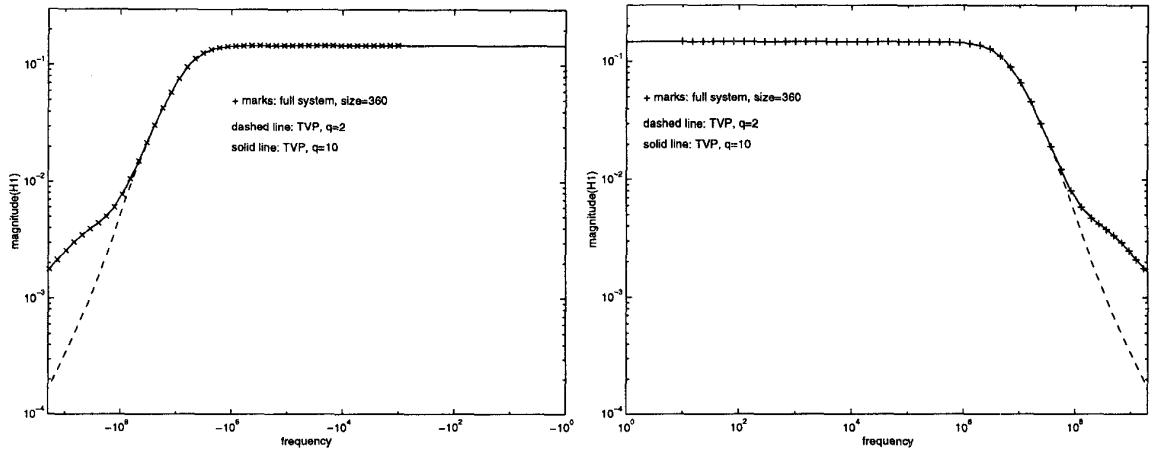

Figure 4: I-channel buffer/mixer $H_1(s)$: TVP vs full system, +ve and -ve frequencies

TVP, $q=2$	TVP, $q=10$
-5.3951e+06	-5.3951e+06
-6.9196e+07 - j3.0085e+05	-9.4175e+06
	-1.5588e+07 - j2.5296e+07
	-1.5588e+07 + j2.5296e+07
	-6.2659e+08 - j1.6898e+06
	-1.0741e+09 - j2.2011e+09
	-1.0856e+09 + j2.3771e+09
	-7.5073e+07 - j1.4271e+04
	-5.0365e+07 + j1.8329e+02
	-5.2000e+07 + j7.8679e+05

Table 2: Poles of $H_1(s)$ for the I-channel buffer/mixer

The clock signal to the SC filter had a time-period of 78ns, but some sections of the circuit were fed at twice that frequency, about 25.6MHz. The steady state waveform of the output node of the circuit (in the absence of input) is shown in Figure 5. The steady state was obtained by time-domain techniques akin to shooting.

The output node did not have switching activity filtered out. Figure 6 depicts a multi-time scale plot of the waveform at the output node in the presence of a 10kHz sinusoidal input. (For details on how to interpret multi-time plots of waveforms, see [Roy98b] or [Roy97a]. For the present purpose, it suffices to use the fact that a cross-section parallel to the signal time scale represents the envelope of the signal riding on the switching variations. By moving these cross-sections to different points along the clock time-scale, the signal envelope at different points of the clock waveform can be chosen). The time-variation of the circuit is apparent from the change in the signal depending on the phase of the fast clock. Note how the sinusoidal signal is transmitted in the region between 60ns and 78ns on the clock time scale, but is cut out (because switches are off) between about 0-20ns and 40ns-60ns. For macromodelling, we chose to sample the output at 70ns on the clock time scale, *i.e.*, in the middle of the clock phase in which the signal is being transmitted. In other words, the transfer function being modelled is that between the input and the waveform obtained by taking a cross-section, parallel to the signal time scale, at 70ns on the clock time scale in Figure 6.

A time-domain version of TVP was applied to reduce this transfer function. Running TVP for the order 10 reduced model took about 10s on a Sun UltraSparc machine. Table 3 shows the poles of the transfer function, obtained from an eigenvalue analysis on reduced models of size 3 and 10 respectively. The dominant pole is at 206kHz, close to the designed value of 200kHz.

Figure 7 depicts the input-to-output transfer functions from the two macromodels. As can be seen, even a tiny behavioral model (of size 3) is sufficient to capture the frequency-response upto well beyond the dominant pole, while a size 10 model details behaviour to frequencies orders of magnitude higher.

TVP, $q=3$	TVP, $q=10$
-2.06e5	-2.06e5
-1.42e6	-1.39e6
-2.64e10	-2.65e6
	-5.22e6
	-2.49e6+j1.29e7
	-2.49e6-j1.29e7
	-1.08e7
	-2.04e7
	-1.16e8
	-7.34e10

Table 3: Poles (in Hz) of switched-capacitor integrator transfer function

4 Conclusion

We have presented applications of TVP, a technique for reduced-order modelling of linear time-varying systems. The technique is useful for macromodelling and hierarchical verification of communication systems, including noise. An RF mixer and a switched-capacitor integrator have been macromodelled with equivalent systems more than two orders of magnitude smaller, resulting in corresponding speedups.

Acknowledgments

We would like to thank Shariar Moinian and David Long for the RFIC circuit, and Peter Kinget for the switched-capacitor integrator.

References

[BWLBG96] H.G. Brachtendorf, G. Welsch, R. Laur, and A. Bunse-Gerstner. Numerical steady state analysis of electronic circuits driven by multi-tone signals. *Electrical Engineering (Springer-Verlag)*, 79:103–112, 1996.

[MFR95] R.C. Melville, P. Feldmann, and J. Roychowdhury. Efficient multi-tone distortion analysis of analog integrated circuits. In *Proc. IEEE CICC*, pages 241–244, May 1995.

[RA92] M. Rösch and K.J. Antreich. Schnell stationäre Simulation nichtlinearer Schaltungen im Frequenzbereich. *AEÜ*, 46(3):168–176, 1992.

[RLF98] J. Roychowdhury, D. Long, and P. Feldmann. Cyclostationary Noise Analysis of Large RF Circuits with Multitone Excitations. *IEEE J. Solid-State Ckts.*, 33(2):324–336, Mar 1998.

[Roy97a] J. Roychowdhury. Efficient Methods for Simulating Highly Nonlinear Multi-Rate Circuits. In *Proc. IEEE DAC*, 1997.

[Roy97b] J. Roychowdhury. Multiple Time Scales for Reduced-Order Modelling of LPTV and Nonlinear Systems. Technical Report ITD-97-32683A, Bell Laboratories, October 1997.

[Roy98a] J. Roychowdhury. Analysing Circuits with Widely-Separated Time Scales using Numerical PDE Methods. *IEEE Trans. Ckts. Syst. – I: Fund. Th. Appl.*, 1998. In press.

[Roy98b] J. Roychowdhury. MPDE methods for efficient analysis of wireless systems. In *Proc. IEEE CICC*, May 1998.

[Roy98c] J. Roychowdhury. Reduced-order modelling of linear time-varying systems. In *Proc. ICCAD*, 1998.

[Roy98d] J. Roychowdhury. TVP: Theory and Implementation, Apr 1998. Bell Laboratories internal memorandum.

[TKW95] R. Telichevesky, K. Kundert, and J. White. Efficient Steady-State Analysis based on Matrix-Free Krylov Subspace Methods. In *Proc. IEEE DAC*, pages 480–484, 1995.

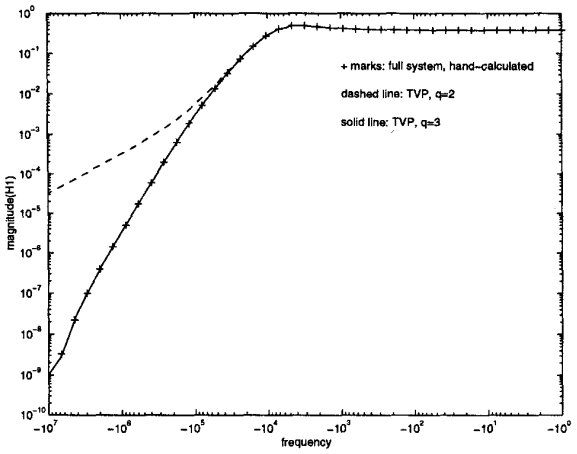

(a) -ve frequencies

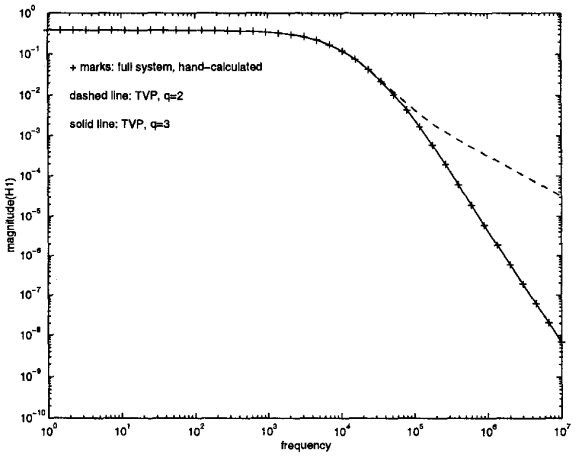

(b) +ve frequencies

Figure 3: Simple circuit: $H_1(s)$ from TVP vs hand-calculations

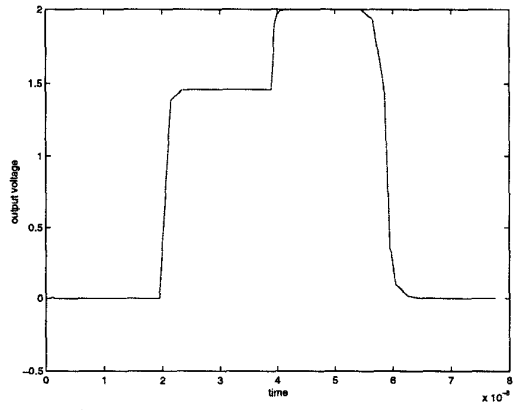

Figure 5: Steady state output of SC integrator (with zero input)

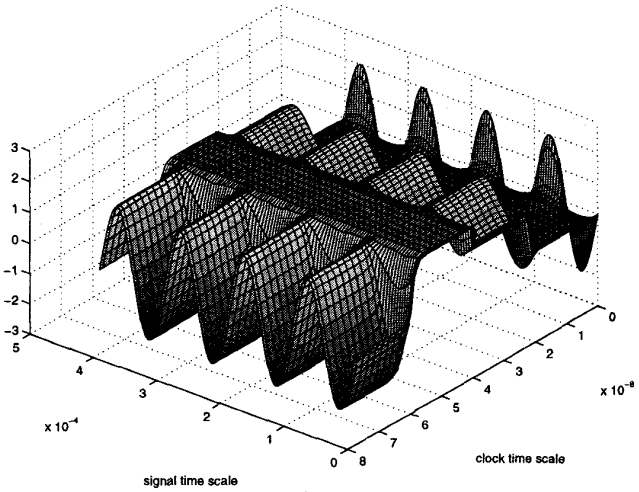

Figure 6: Multi-time output waveform of SC integrator

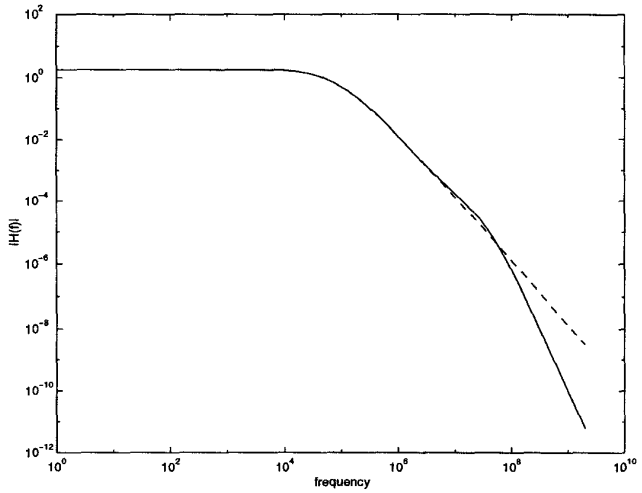

Figure 7: Frequency response of SC macromodels